scientific reports

Check for updates

OPEN

Talin2 binds to non-muscle myosin IIa and regulates cell attachment and fibronectin secretion

Xiaochuan Wang[1]✉, Zbigniew Baster[2,3], Latifeh Azizi[4,5], Liqing Li[2], Zenon Rajfur[3,6], Vesa P. Hytönen[4,5]✉ & Cai Huang[2,7]✉

Talin2 is localized to large focal adhesions and is indispensable for traction force generation, invadopodium formation, cell invasion as well as metastasis. Talin2 has a higher affinity toward β-integrin tails than talin1. Moreover, disruption of the talin2-β-integrin interaction inhibits traction force generation, invadopodium formation and cell invasion, indicating that a strong talin2-β-integrin interaction is required for talin2 to fulfill these functions. Nevertheless, the role of talin2 in mediation of these processes remains unknown. Here we show that talin2 binds to the N-terminus of non-muscle myosin IIA (NMIIA) through its F3 subdomain. Moreover, talin2 co-localizes with NMIIA at cell edges as well as at some cytoplasmic spots. Talin2 also co-localizes with cortactin, an invadopodium marker. Furthermore, overexpression of NMIIA promoted the talin2 head binding to the β1-integrin tail, whereas knockdown of NMIIA reduced fibronectin and matrix metalloproteinase secretion as well as inhibited cell attachment on fibronectin-coated substrates. These results suggest that talin2 binds to NMIIA to control the secretion of extracellular matrix proteins and this interaction modulates cell adhesion.

Keywords Talin2, Non-muscle myosin IIA, Fibronectin secretion, MMP1, Talin-integrin interaction, Cell adhesion

Talin is a β-integrin- and actin-binding protein that controls integrin activation and focal adhesion assembly[1–3]. Talin is a 250 kDa protein with an amino-terminal head domain and a carboxy-terminal rod domain[4,5]. Its head contains a FERM domain, which is responsible for talin binding to β-integrin tails and the consequent integrin activation[1,6], while its rod domain comprises several vinculin-binding sites, and two actin-binding sites[7–9], which provide a linkage between the integrin and actin filaments, where the latter binds NMIIA.

There are two variants of talin protein: talin1 and talin2. Talin1 is usually found at smaller focal adhesions, often in the peripheral region of cells[10,11]. This localization is consistent with the role of talin1 in cell migration and mechanical sensing. Talin2 is usually found at large focal adhesions and fibrillar adhesions in the central areas of cells[10–12], a site for fibronectin secretion and invadopodium formation[11,13]. Although talin1 has been extensively studied, the biological function of talin2 is less understood. Our recent studies show that talin2 is localized to large focal adhesions and indispensable for traction force generation, invadopodium formation, cell invasion as well as metastasis[11,14,15]. Using biochemical assays with peptides, Anthis et al. found that the β1D binds talin2 with higher affinity than talin1[16]. Using GST-pull-down assays, we found that talin2 binds to β1A-, β1D- and β3-integrin tails more efficiently than talin1[11,17]. Moreover, disruption of the talin2-β-integrin interaction inhibits traction force generation, invadopodium formation and cell invasion, indicating that a strong talin2-β-integrin interaction is required for talin2 to fulfill these functions[11,14]. Talin2 also mediates MMP secretion[18], which is consistent with its role in invadopodium formation. Nevertheless, the molecular mechanism by which talin2 mediates these functions remains unknown.

Non-muscle myosin IIA (NMIIA) is the major myosin involved in force generation[19,20], which in turn regulates integrin activation[21–24]. It is generally believed that NMIIA transmits force from F-actin to the extracellular

[1]The Second Hospital of Shandong University, Jinan 250033, Shandong, China. [2]Markey Cancer Center, University of Kentucky, Lexington, KY 40506, USA. [3]Institute of Physics, Faculty of Physics, Astronomy and Applied Computer Science, Jagiellonian University, 30-348, Kraków, Poland. [4]Faculty of Medicine and Health Technology, Tampere University, 33520 Tampere, Finland. [5]Fimlab Laboratories, Tampere, Finland. [6]Jagiellonian Center of Biomedical Imaging, Jagiellonian University, 30-348, Kraków, Poland. [7]Present address: Doer Biologics Inc, 2nd Floor, Building 3, Hexiang Science and Technology Center, Medicine Port Town, Qiantang District, Hangzhou, Zhejiang Province, China. ✉email: 2019120219@mail.sdu.edu.cn; vesa.hytonen@tuni.fi; caihuang@doerbio.com

matrix through talin. Talin, as mentioned earlier, interacts with β-integrin tails and F-actin through its head and rod domains, respectively[24,25]. NMIIA is deregulated in various types of cancers and is involved in the stemness of hepatocellular carcinoma cells, the chemosensitivity of colorectal cancer cells and the resistance of breast cancer cells to neratinib, a pan-HER inhibitor[26–31]. Depletion of the NMIIA heavy chain suppressed cell growth, proliferation, migration, invasion, and metastasis, suggesting a key role of NMIIA in tumor progression. However, the molecular mechanism whereby NMIIA regulates these processes remains to be elucidated.

In the present study, we show that talin2 binds to the N-terminus of NMIIA through its F3 subdomain. Moreover, talin2 co-localizes with NMIIA at cell edges as well as at some cytoplasmic spots. Furthermore, overexpression of NMIIA promoted talin2 head binding to the β1 integrin tail, whereas knockdown of NMIIA reduced fibronectin secretion as well as cell attachment on fibronectin. Thus, talin2 may mediate cancer cell invasion and metastasis by interacting with NMIIA. NMIIA may transmit forces through an NMIIA-talin2-integrin axis, which could be a novel molecular mechanism by which NMIIA mediates integrin activation and controls traction force generation.

Materials and methods

All experimental methods and protocols were performed in accordance with the relevant guidelines and regulations of the University of Kentucky and Tampere University, and the database analysis was approved by the ethnic regulation committee of The Second Hospital of Shandong University. Human subjects are not involved in this study.

Reagents

Anti-NMIIA rabbit polyclonal antibody (#3403) was from Cell Signaling Technology. Anti-cortactin mouse monoclonal antibody (clone 4F11) was from EMD Millipore. Anti-talin2 (clone 53.8) antibody was from AbD Serotec. Anti-Integrin beta 1 antibody [12G10] was from Abcam (Waltham, MA). Anti-MMP9 rabbit polyclonal antibody (A0289) was from ABclonal (Woburn, MA). Anti-collagen Type I monoclonal (clone COL-1), anti -MMP1 monoclonal (clone 41-1E5) and anti-tubulin (clone B-5-1-2) monoclonal antibodies were from Sigma. Anti-fibronectin monoclonal antibody (SKU: MA1116), Alexa Fluor 633 phalloidin and DyLight 488 conjugated goat anti-mouse IgG (H + L) were from Thermo Scientific. DyLight 550 or 633 labeled goat anti-mouse and anti-rabbit IgG (H + L) were from Immunoreagents (Raleigh, NC). Fibronectin was from Akron Biotech. Pfu Ultra was from Agilent Technologies. Laminin (L2020), Duolink® In Situ PLA® Probe Anti-Mouse MINUS (DUO92004) and Duolink® In Situ PLA® Probe Anti-Rabbit PLUS (DUO92002) were from Sigma. Cold Fusion Cloning Kit was from System Biosciences (Palo Alto, CA). Anti-GFP monoclonal antibody and Safectine RU50 transfection kit were purchased from Syd Labs (Malden, MA). DNA primers were synthesized by Integrated DNA Technologies.

Plasmid construction

The full-length pGFP-NMIIA was a gift from Robert Adelstein (Addgene plasmid # 11347)[32]. pQE-talin1$_{1–446}$, pQE-Talin2$_{1–449}$, pEGFP-talin2$_{1–449}$^{WT}, and the full-length pEGFP-talin2 WT were described previously[17]. pGEX-talin2$_{90–403}$, pGEX-talin2$_{206–316}$, and pGEX-talin2$_{90–316}$ were generated by amplifying DNA fragments encoding talin2 residues 90–403, 206–316, and 90–316 using oligo pairs 1/2, 3/4, and 1/4 (Table 1) as primers, respectively, digesting the DNA products with BamH1/Sal1 and subcloning into pGEX-4T-1 vector. pEGFP-NMIIA$_{Δ213–1897}$ was constructed by digesting pGFP-NMIIA with PstI and circularizing the largest fragment. pEGFP-NMIIA$_{Δ213–1960}$ was created by digesting pGFP-NMIIA with PstI/SalI, treating with Klenow, and circularizing the largest fragment. pEGFP-NMIIA$_{Δ1–1811}$ was generated by digesting pGFP-NMIIA with XhoI and circularizing the largest fragment. pEGFP-NMIIA$_{Δ1–1340}$ were constructed by digesting pGFP-NMIIA with HindIII/EcoRI, treating with mung bean nuclease and circularizing the largest fragment. NMIIA shRNA1 and shRNA 2, targeting base pairs 3235–3255 and 2428–2448 of NM002473.6, respectively, were produced by annealing and subcloning oligo pairs 5/6 and 7/8 into pLKO.1 vector, respectively (Table 1)). All plasmids were sequenced by Eurofins MWG Operon (Huntsville, AL).

Oligo no.	Oligo sequences
1	5′-ATC TAG GAT CCG CGT GTC GAG TCA TTC GGG AAC G-3′
2	5′-ATA TAT GTC GAC CTA CAG GAT GAT GTC AAT GTA GCC TGC AAT C-3′
3	5′-TTA CAG GAT CCG TAG ATT CGA GAG ACC CCG TGC AG-3′
4	5′-AAT AGG TCG ACT AGA AGA AGG ACA CGC CAT ATG TGC GG-3′
5	5′-CCG GGC CAA GCT CAA GAA CAA GCA TCT CGA GAT GCT TGT TCT TGA GCT TGG CTT TTT G-3′
6	5′-AAT TCA AAA AGC CAA GCT CAA GAA CAA GCA TCT CGA GAT GCT TGT TCT TGA GCT TGG C-3′
7	5′-CCG GGA CAG CAA TCT GTA CCG CAT TCT CGA GAA TGC GGT ACA GAT TGC TGT CTT TTT G-3′
8	5′ -AAT TCA AAA AGA CAG CAA TCT GTA CCG CAT T CT CGA GAA TGC GGT ACA GAT TGC TGT C-3′

Table 1. Oligos used in the study.

Cell culture and transfection

CHO-K1 Chinese hamster ovary cells, 293T human embryonic kidney cells, MDA-MB-231 human breast cancer cells, and U2 OS human bone osteosarcoma cells were from the American Type Culture Collection and were maintained in DMEM medium (Corning Inc.) containing 10% fetal bovine serum (FBS), penicillin (100 U/ml) and streptomycin (100 µg/ml). CHO-K1 and 293T cells were transfected with Safectine RU50 according to the manufacturer's protocol. MDA-MB-231 human breast cancer cells were transfected with Lipofectamine LTX with Plus Reagent according to the manufacturer's protocol.

The TLN1$^{-/-}$ TLN2$^{-/-}$ mouse kidney fibroblast (MKF) cell line was a gift from Reinhard Fässler's Laboratory (Max Planck Institute of Biochemistry, Germany)[33]. The cell line was cultured in high glucose Dulbecco's modified Eagle medium (DMEM) supplemented with 10% fetal bovine serum (FBS), and maintained in a humidified 37 °C, 5% CO_2 incubator. Regular mycoplasma contamination tests were performed on the cell line. To re-express talin in this cell line, talin expression constructs were based on human talin1 (BC042923) and human talin2 (NM015059) and talins were fused with yellow fluorescent protein (YPet) as described earlier[15]. For transfection, cells were exposed to 6 µg of plasmid DNA per 10^6 cells using the Neon transfection system (Thermo Fisher Scientific) with the following parameters: 1400 V, 30 ms, one pulse.

NMIIA knockdown

The preparation of viruses and cell infection were performed as described previously[34,35]. NMIIA shRNAs were co-transfected with packaging vectors pMDLg/pRRE, pRSV-Rev, and CMV-VSVG into 293T cells. Lentiviral particles were collected and used to infect U2 OS and MDA-MB-231 cells. The cells were selected with puromycin for 2 weeks. The NMIIA expression was detected by Western blotting using an anti-NMIIA polyclonal antibody.

Protein interaction assays

CHO-K1 cells were transfected with different constructs where indicated. At 28 h post-transfection, the cells were harvested in lysis buffer A (50 mM Tris–HCl pH 7.4, 1% NP-40, 150 mM NaCl, 1 mM EDTA, and a protease inhibitor cocktail). Cell lysates were cleared by centrifugation and incubated with purified His-tagged proteins as indicated and glutathione-Sepharose beads loaded with GST or GST-β1A-integrin tails at 4 °C for 2 h. The beads were washed with the lysis buffer 4 times and resuspended in SDS-sample buffer. Samples were analyzed using SDS-PAGE and transferred to nitrocellulose membrane for the detection of interacting proteins.

Mass spectrometry

A 250-kD protein band was excised from the Coomassie blue-stained gel (Fig. 1A), destained, cut into small pieces, and then digested with sequencing-grade modified trypsin at 37 °C overnight. The resulting peptides

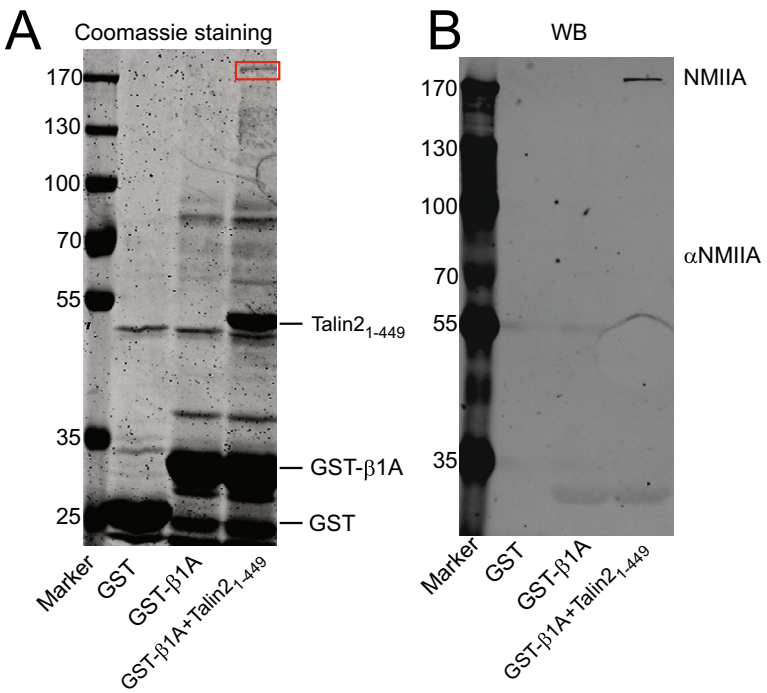

Fig. 1. NMIIA was co-precipitated with talin2. Glutathione agarose beads preloaded with GST- β1A tail or GST were incubated with U2 OS cell lysates in the absence and presence of His-tagged talin2$_{1–449}$ (5 µg). The bound proteins were detected using Coomassie blue staining (**A**). The protein band in the red rectangle was analyzed using mass spectrometry (Table 1). The identity of the protein was then verified by an anti-NMIIA rabbit polyclonal antibody (**B**).

were analyzed by LC–MS/MS using an LTQ-Orbitrap mass spectrometer. The identities of detected m/z + 2 ions were further analyzed by MS/MS spectra.

Computational modeling

Protein structural models were generated using the AlphaFold2.3.2 protein structure prediction module, and protein–protein interaction models were constructed using the Frodock protein docking module 2.0 (https://frodock.iqf.csic.es/) as described in Supplementary information.

Immunofluorescence staining and confocal imaging

MDA-MB-231 cells were plated on glass coverslips that were precoated with 5 μg/ml fibronectin or laminin as indicated. The cells were then transfected where indicated using Lipofectamine Plus. At 24 h post transfection, for immunofluorescence staining, the cells were fixed with 4% paraformaldehyde, permeabilized with 0.5% Triton X-100, blocked with 5% BSA in PBS, and then incubated with primary antibodies. Unbound primary antibodies were washed away using DPBS. The stained samples were then visualized by incubating with fluorescent-conjugated secondary antibodies. The staining and EGFP fluorescence were viewed by using a Nikon Eclipse Ti2 A1 confocal microscope equipped with a Plan Apo λ 100× Oil Immersion 4x, 1.45 NA objective or a Nikon Eclipse Ti TIRF microscope equipped with a 60×, 1.45 NA objective. Images were acquired using NIS-Elements (Nikon) and analyzed with Fiji ImageJ[36]. Before analysis, z-stack images were deconvolved using Batch Deconvolution Fiji plugin[37] with Richardson-Lucy deconvolution algorithm. Point spread function (PSF) was calculated using Gibson-Lanni PSF model with the highest accuracy and parameters matching acquisition. Pearson and Spearman colocalization coefficients between NMIIA and talin2 were generated using Coloc2 software in Fiji (https://imagej.net/plugins/coloc-2). 2D colocalization histogram was generated using 'Colocalization Threshold' function in Fiji.

To analyze talin/NMIIA co-localization in talin-rescued MKF cells, transfected cells were incubated overnight on coverslips coated with 10 μg/ml human fibronectin. Following incubation, cells were fixed with 4% paraformaldehyde, permeabilized, and immune-stained using a standard protocol. The antibody used for immunostaining against NMIIA was Myosin IIA antibody (Cell Signaling Technology #3403, 1:50). Alexa Fluor 568 goat anti-rabbit IgG (Life Technologies A11011; 1:200) was used as the secondary antibody. Immunostained samples were imaged using a Zeiss LSM800 laser scanning confocal microscope, mounted on an inverted Zeiss Axio Observer.Z1 (Zeiss, Oberkochen, Germany) with a Plan-Apochromat 63×/1.40, WD 0.19 mm oil immersion objective. To quantify adhesion-localized protein intensity, we selected 10 adhesion sites per cell from the stack with the brightest talin adhesion intensities based on the Ypet-talin channel. Each selection was copied to the red fluorescence channel, followed by intensity measurement from both channels using ImageJ.

For active integrin staining, U2 OS cells were plated on glass coverslips that were precoated with 5 μg/ml fibronectin. The cells were then transfected using Lipofectamine Plus. At 24 h post transfection, the cells were fixed with paraformaldehyde, permeabilized with Triton X-100, blocked with BSA in PBS, and then sequentially incubated with an anti-active-β-integrin antibody (12G10) and a Dylight 550-labeled goat anti-mouse antibody. The staining and EGFP fluorescence were viewed using a Nikon Eclipse Ti TIRF microscope equipped with a 60×, 1.45 NA objective. Images were acquired using NIS-Elements (Nikon) and the staining intensity and adhesion area were analyzed using Fiji ImageJ[36].

Proximity ligation assay (PLA)

PLA was performed according to a protocol from the manufacturer. Briefly, cells on coverslips were fixed with 4% paraformaldehyde, permeabilized, and blocked with a blocking buffer. The cells were incubated with primary antibodies (anti-talin2 mouse mAb and anti-NMIIA rabbit pAb, or anti-talin2 mouse mAb only in the control sample). After washing, cells were incubated with PLA Plus probe and Minus probe. The coverslips were washed to remove unbound probes, and were incubated with T4 ligase in a ligation buffer. The coverslips were then washed and incubated with an amplification solution (with oligonucleotide probes labeled with fluorophore) and a DNA polymerase to amplify the ligation product. The coverslips were washed, mounted on slides using a mounting medium with DAPI, and then viewed with a Nikon confocal microscope.

Protein secretion assays

MDA-MB-231 cells were cultured in normal culture media (10% FBS) to 80% confluence. The cells were washed 3 times with PBS and then cultured in serum-free DMEM media including 20 ng/ml HGF for 24 h. The media were collected, concentrated using Spin-X ultrafiltration concentrators (10,000 Da cut-off), and then analyzed for the secretion of fibronectin, collagen, MMP1, and MMP9 by Western blotting.

Database analysis

To analyze gene expression, in the OncoDB website (https://oncodb.org/), "Expression profile" tab was selected under "Expression analysis" tab on the left panel, the gene symbol and the cancer types to be analyzed were provided. The gene expression levels (mRNA levels) in the cancer vs normal tissues were plotted. To analyze the expression correlation between two genes, "Correlation of Expression" tab under "Expression analysis" tab on the left panel was selected and the analysis was performed following the instructions on the website.

Results

We have previously demonstrated that talin2 is essential for tumor growth and metastasis[14]. We analyzed the gene expression pattern of talin2 in cancers compared with normal tissues using OncoDB (http://oncodb.org)[38], an online database that integrates RNA-seq, DNA methylation, and related clinical data from over 10,000 cancer patients in the TCGA study as well as from normal tissues in the GTEx study to identify abnormal patterns in gene expression in cancer. As shown in Supplementary Fig. S1, the expression of talin2 is up-regulated in cancer tissues of 42% of cancer types examined compared with the normal tissues, including pancreatic adenocarcinoma (PAAD), cholangiocarcinoma (CHOL), stomach adenocarcinoma (STAD), and lung squamous cell carcinoma (LUSC), prostate cancer (PRAD) and liver hepatocellular carcinoma (LIHC). In addition, it is also overexpressed in some cases of other cancer types, such as head and neck squamous cell carcinomas (HNSC). Since fibroblasts express high levels of talin2, it is unknown whether this overexpression results from tumor cells or stromal cells. However, it has been well demonstrated that talin2 expression in breast cancer tissues is much higher than that in normal tissues[39,40]. In conclusion, talin2 is up-regulated in several types of cancer, which is consistent with its role in tumor growth and metastasis[14].

Previously we demonstrated that the binding of talin2 to β1-integrin mediates cancer invasion[11,14]. To identify proteins that potentially regulate talin2-β1-integrin interaction, GST-β1A-integrin tails were incubated with lysates of U2 OS cells, which express high level of talin2, in the absence or presence of His tagged talin2$_{1–449}$. A 250 kDa protein was specifically enriched with talin2$_{1–449}$ (Fig. 1A). This protein was identified as NMIIA using mass spectrometry (Table 2) as described in the Methods section and verified using Western blotting (Fig. 1B). In GST-β1-integrin tail pulldown assays, NMIIA was efficiently pulled down by GST-β1 integrin tail in the presence of talin2$_{1–449}$, but only a very faint band was observed in the presence of talin1$_{1–443}$ (Fig. 2A). GST did not obviously pull down NMIIA. This result suggests that NMIIA is a potential talin2-binding partner.

To know whether endogenous talin2 interacts with NMIIA in cancer cells, we immunoprecipitated talin2 from U2 OS cells using an anti-talin2 mouse monoclonal antibody and detected the co-immunoprecipitation of NMIIA (Fig. 2B), suggesting that NMIIA is a talin2-binding protein.

To know which subdomain of the talin2 head binds to NMIIA, different truncated mutants with F_0, F_1, and (or) F_3 deletion were generated (Fig. 2C) and used for binding assays. The cell lysates of CHO-K1 cells transiently transfected with NMIIA-GFP were incubated with GST-β1-integrin tail/His-talin2$_{1–449}$, GST-talin2$_{90–403}$, GST-β1-integrin tail, and GST, respectively, and the bound NMIIA was detected with an anti-GFP antibody. Either GST-talin2$_{90–403}$ or GST-β1A/Talin2$_{1–449}$ complex bound to NMIIA, whereas GST and GST-β1-integrin tail alone did not (Fig. 2D), suggesting that the talin2 head domain binds to NMIIA independent of the β1-integrin. To know which subdomain of talin2 interacts with NMIIA, the cell lysates of CHO-K1 cells transiently transfected with NMIIA-GFP were incubated with GST-talin2$_{206–316}$, -talin2$_{90–403}$, -talin2$_{90–316}$ or GST, and their binding to NMIIA was examined. As shown in Fig. 2E, only GST-talin2$_{90–403}$ was able to bind to NMIIA, while GST-talin2$_{206–316}$, -talin2$_{90–316}$ and GST showed no binding, suggesting that residues 317–403 (F_3 subdomain) are required for talin2 binding to NMIIA.

NMIIA is composed of a highly conserved motor domain, a lever arm and a tail domain. In addition, the N-terminus of NMIIA also contains a SH3-like domain and its function is unknown[41,42]. We hypothesized that NMMIIA binds to talin2 through its N-terminal or C-terminal ends. To determine which regions of NMIIA are responsible for talin2 binding, different truncated NMIIA mutants with deletion at the N-terminus, C-terminus, or central region, including EGFP-NMIIA$_{Δ214–1897}$, -NMIIA$_{Δ214–1960}$, -NMIIA$_{Δ1–1813}$, and -NMIIA$_{Δ1–1337}$ were generated (Fig. 3A), transiently transfected into CHO-K1 cells, and the cell lysates were used to examine the interaction of these deletion mutants with GST-talin2$_{90–403}$ by pulldown assays. NMIIA$_{Δ214–1897}$ and NMIIA$_{Δ214–1960}$ bound to talin2 efficiently, whereas NMIIA$_{Δ1-1813}$ and NMIIA$_{Δ1–1337}$ showed only a faint binding to talin2 (Fig. 3B, C), suggesting that residues 1–213 of NMIIA are mainly responsible for talin2 binding. Because of the weak binding of NMIIA$_{Δ1–1813}$ and NMIIA$_{Δ1–1337}$, the possibility that there exists another weak binding site for talin at the C-terminus of NMIIA is not ruled out.

We performed computational modeling of talin1$_{1–400}$/NMIIA$_{1–230}$ and talin2$_{1–403}$/NMIIA$_{1–230}$ interaction. The structural models of talin1$_{1–400}$, talin2$_{1–403}$ and NMIIA$_{1–230}$ were generated using AlphaFold2.3.2, and the complex models were constructed using FRODOCK protein docking software. As shown in Supplementary Fig. S2, talin1$_{1–400}$ interacts with NMIIA$_{1-230}$ through its F_0 subdomain, whereas talin2$_{1–403}$ binds to NMIIA$_{1–230}$ through its F_0 and F_3 subdomains. Complex interface analysis shows that there are 22 talin1 and 34 talin2 residues involved

Peptide sequences	m/z + 2	Residues on NMIIA
NFINNPLAQADWAAK	837.192	15–29
TDLLLEPYNK	603.804	290–299
QEEEMMAK	498.454	843–850
LSLSTK	324.924	1325–1330
DLEGLSQR	459.103	1393–1400
ALSLAR	315.373	1478–1483
ANLQIDQINADLNLER	920.725	1755–1770
IAQLEEQLDNETK	766.832	1816–1828

Table 2. Sequences of peptides identified from a talin2-bing protein band by mass spectrometry.

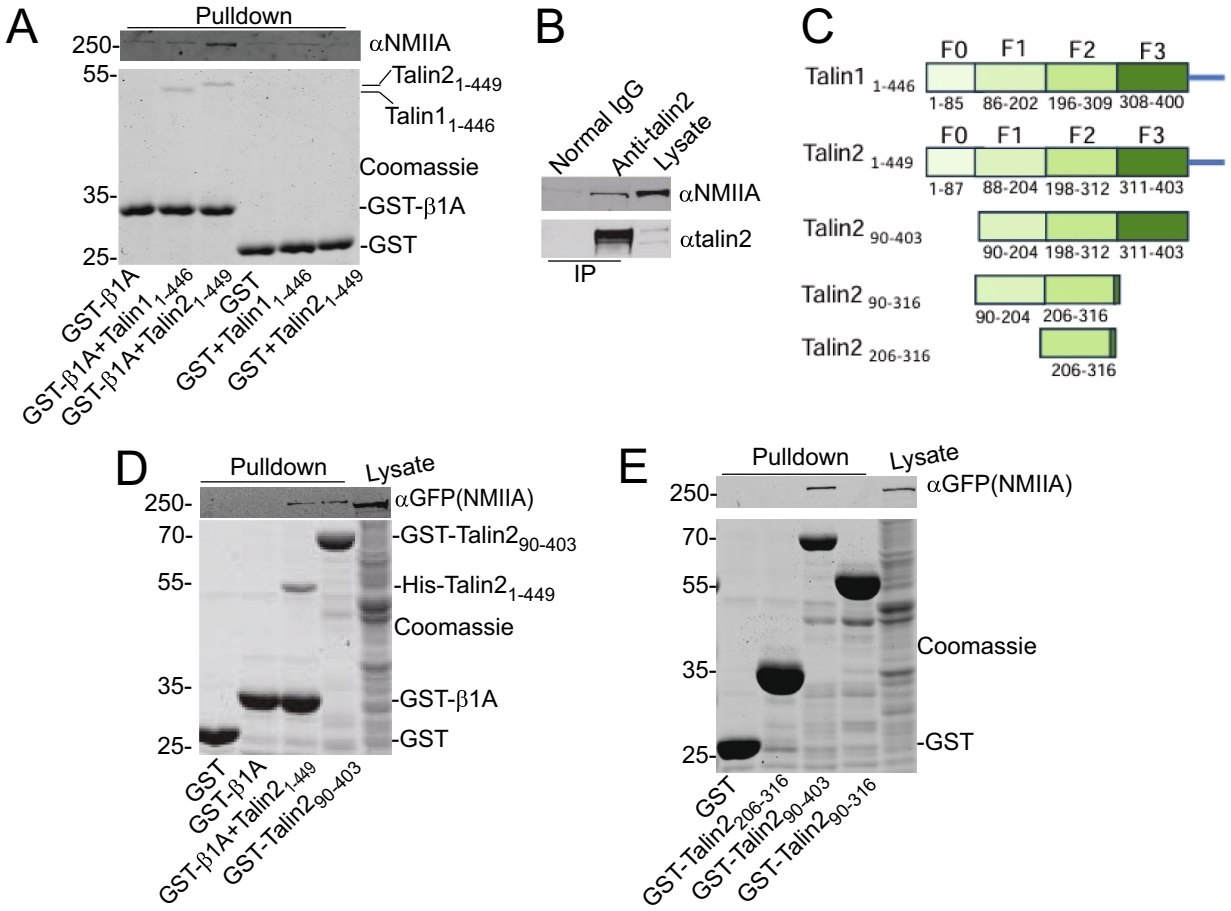

Fig. 2. Talin2 interacts with NMIIA. (**A**) NMIIA was co-precipitated with talin2 in GST-β1-integrin tail pulldown assays. Glutathione agarose beads preloaded with GST-β1A tail or GST were incubated with U2 OS cell lysates in the absence and presence of His-tagged talin1$_{1-446}$ or talin2$_{1-449}$ (5 μg). The bound NMIIA was detected using an anti-NMIIA rabbit polyclonal antibody. (**B**) Co-immunoprecipitation of talin2 with NMIIA. U2 OS cell lysates were immunoprecipitated with normal IgG or an anti-talin2 mouse monoclonal antibody. The co-immunoprecipitation of NMIIA was detected using the anti-NMIIA polyclonal antibody. (**C**) Schematic domain structures of talin2 mutants used in the experiments. (**D**) Binding of NMIIA to talin2. Glutathione agarose beads preloaded with GST, GST-β1A tail or GST-talin2$_{90-403}$ (5 μg) were incubated with the lysates of CHO-K1 cells expressing EGFP-NMIIA. GST-β1A tails were also incubated with the cell lysate in the presence of His-tagged talin2$_{1-449}$ (5 μg). The bound NMIIA was detected using an anti-GFP mouse monoclonal antibody. (**E**) Glutathione agarose beads preloaded with GST, GST-talin2$_{206-316}$, -talin2$_{90-403}$, or -talin2$_{90-316}$ were incubated with CHO-K1 cell lysates with overexpressed EGFP-NMIIA.

in the talin1$_{1-400}$/NMIIA$_{1-230}$ and talin2$_{1-403}$/NMIIA$_{1-230}$ interaction, respectively. This computational data further supports that talin2 binds NMIIA more efficiently than talin1.

We previously showed that talin2 plays a key role in the invasion and metastasis of MDA-MB-231 cells[11,14]. To examine if talin2 co-localizes with NMIIA, MDA-MB-231 cells were transfected with EGFP-talin2 and stained with an anti-NMIIA antibody and phalloidin. As shown in Fig. 4A and Supplementary Fig. S3, talin2 co-localized with NMIIA at cell edges as well as at some centered spots. We also analyzed the co-localization between talin2 and NMIIA using a 2D histogram, and quantified the correlation between talin2 and NMIIA using Pearson (r_p) and Spearman (r_s) coefficients. Our analysis shows a high degree of correlation between these two proteins (> 0.6) (Fig. 4B), confirming the co-localization between talin2 and NMIIA. Because of the key role of talin2 in invadopodium formation[11], we tested the co-localization of talin2, NMIIA and cortactin, an invadopodium marker[43,44]. To this end, MDA-MB-231 cells were transiently transfected with EGFP-talin2, plated on laminin (Sigma), and stained for NMIIA and cortactin. NMIIA co-localized with talin2 and cortactin at invadopodium-like points (Fig. 4C), suggesting that NMIIA may regulate invadopodium formation/maturation. To further demonstrate the proximity of talin2 with NMIIA in cells, MDA-MB-231 cells were co-incubated with an anti-NMIIA rabbit polyclonal antibody and an anti-talin2 mouse monoclonal antibody, and the proximity between talin2 and NMIIA was determined by a PLA assay. As shown in Fig. 4D, the PLA staining was heavily observed at perinuclear areas as well as cell edges, while there was no visible signal detected when the talin2 antibody was omitted, suggesting a proximity between talin2 and NMIIA in cells, and providing additional support for the interaction of talin2 with NMIIA.

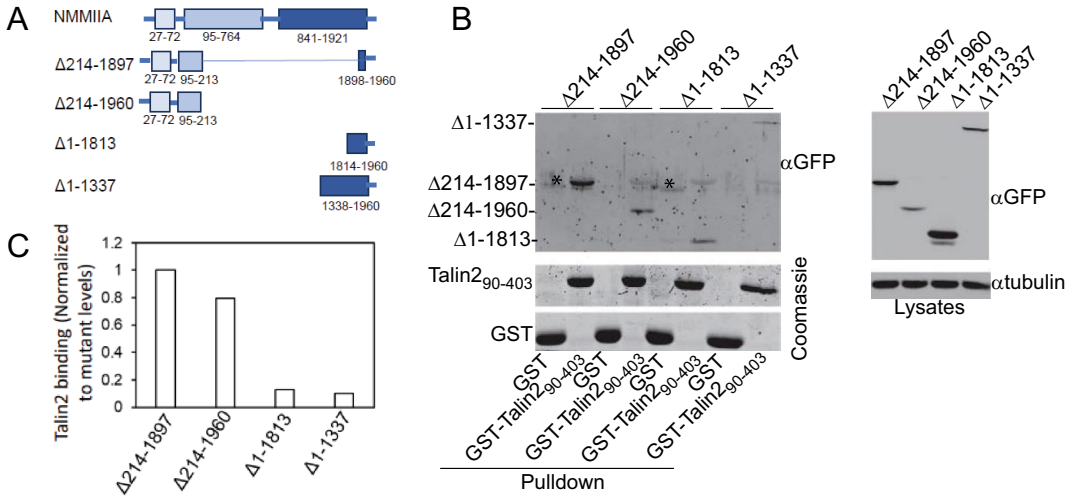

Fig. 3. Truncated NMIIA mutants interacted with talin2. (**A**) Schematic domain structures of NMIIA mutants used in this experiment. (**B**, **C**) Glutathione agarose beads preloaded with GST or GST- talin2$_{90-403}$ were incubated with cell lysates of CHO-K1 cells that express EGFP-NMIIA$_{\Delta214-1897}$, -NMIIA$_{\Delta214-1960}$, -NMIIA$_{\Delta1-1813}$, and -NMIIA$_{\Delta1-1337}$, respectively. The bound NMIIA mutants were detected using the GFP antibody (**B**, left panel). The expression levels of NMIIA mutants were shown in the right panel of (**B**). (**C**) The graph represents the talin2 bound NMIIA mutants that was normalized by NMIIA expression levels. The graph represent the mean from two independent experiments.

To compare talin1 and talin2 co-localization with NMIIA in fibroblasts, the TLN1$^{-/-}$ TLN2$^{-/-}$ mouse kidney fibroblast (MKF) cells were transfected with talin1-YPet or talin2-YPet, and stained with an anti-NMIIA antibody. Re-expressed talin2 exhibited some co-localization with NMIIA in the TLN1$^{-/-}$ TLN2$^{-/-}$ MKF cells, while talin1 showed less co-localization with NMIIA (Fig. 5; Supplementary Fig. S4). Nevertheless, we did not observe such apparent co-localization between talin2 and NMIIA as seen in MDA-MB-231 cells. The observation that the NMIIA/Talin2 ratio is significantly higher than the NMIIA/Talin1 ratio in the adhesion sites suggests that there may be a preferential association or interaction between NMIIA and talin2 compared to NMIIA and talin1. This could imply a specific role of NMIIA in regulating talin2 function.

One of the most important roles of talin is binding to β-integrin tails and consequently activating integrins. To examine if NMIIA regulates talin2 binding to β-integrin, EGFP-talin2$_{1-449}$ was co-transfected with different amounts of EGFP-NMIIA head into CHO-K1 cells, and the binding of EGFP-talin2$_{1-449}$ to GST-β1A-integrin tails was examined by GST pulldown assays. Transfection of NMIIA head significantly promoted the talin2-β1A tail interaction (Fig. 6A). To know the role of NMIIA in cell adhesions, NMIIA-depleted U2 OS cells were plated in FN-coated 96-well plates for 1 h. Unattached cells were washed away and the remaining cells were fixed and stained. Depletion of NMIIA significantly inhibited cell attachment to fibronectin (Fig. 6B), suggesting that NMIIA may regulate integrin activation.

To examine the effect of the truncated NMIIA forms on integrin activation, U2 OS cells were transfected with EGFP-NMIIA$_{\Delta1-1813}$, -NMIIA$_{\Delta214-1894}$, and EGFP empty vector, respectively, plated on fibronectin-coated glass-bottom dishes, and stained with an anti-active-β1-integrin antibody. As shown in Fig. 7, NMIIA$_{\Delta214-1897}$ caused an increase in active β1 integrin staining (Fig. 7A, and B) and promoted cell spreading, whereas NMIIA$_{\Delta1-1813}$ caused a decrease in both (Fig. 7A and C), as compared to an EGFP empty vector. These results suggest that the N-terminus of NMIIA could be involved in the β1 integrin activation.

We showed previously that talin2 mediates the secretion of matrix metalloproteinases (MMP)[18]. Therefore, we set out to examine whether NMIIA knockdown also influences MMP secretion. NMIIA in MDA-MB-231 cells was depleted using shRNAs (Fig. 8A). The NMIIA-depleted cells and the cells infected with the empty vector pLKO.1 were cultured in serum-free media for 24 h, which were then collected and concentrated. MMP in the concentrated media was determined using Western blotting. NMIIA knockdown significantly inhibited MMP1 and MMP9 secretion (Fig. 8B, C). This is consistent with our result showing that talin2 knockdown has significant effects on MMP1 and MMP9 secretion (Supplementary Fig. S5). Surprisingly, NMIIA knockdown also significantly inhibited the secretion of fibronectin, but not that of collagen I (Fig. 8B, C). We recognize that there are inconsistent effects between shRNA 1 and 2 on the NMIIA knockdown and fibronectin secretion, which could have been caused by an off-target effect of shRNAs. Nevertheless, these results suggest that talin2 may mediate fibronectin and MMP secretion through NMIIA.

Next, we analyzed the gene expression pattern of NMIIA in cancers in which talin2 expression was upregulated, compared with normal tissues using OncoDB. As shown in Supplementary Fig. S6, the expression of MYH9 is up-regulated in cancer tissues from 44% of cancer types including PAAD, CHOL, STAD, HNSC, PRAD and LIHC (Supplementary Fig. S6), in which talin2 is also upregulated. This prompted us to examine the correlation between talin2 and NMIIA expression in cancer tissues. Surprisingly, the expression level of talin2 is positively correlated with that of NMIIA in cancer tissues of almost all cancer types examined, except CHOL

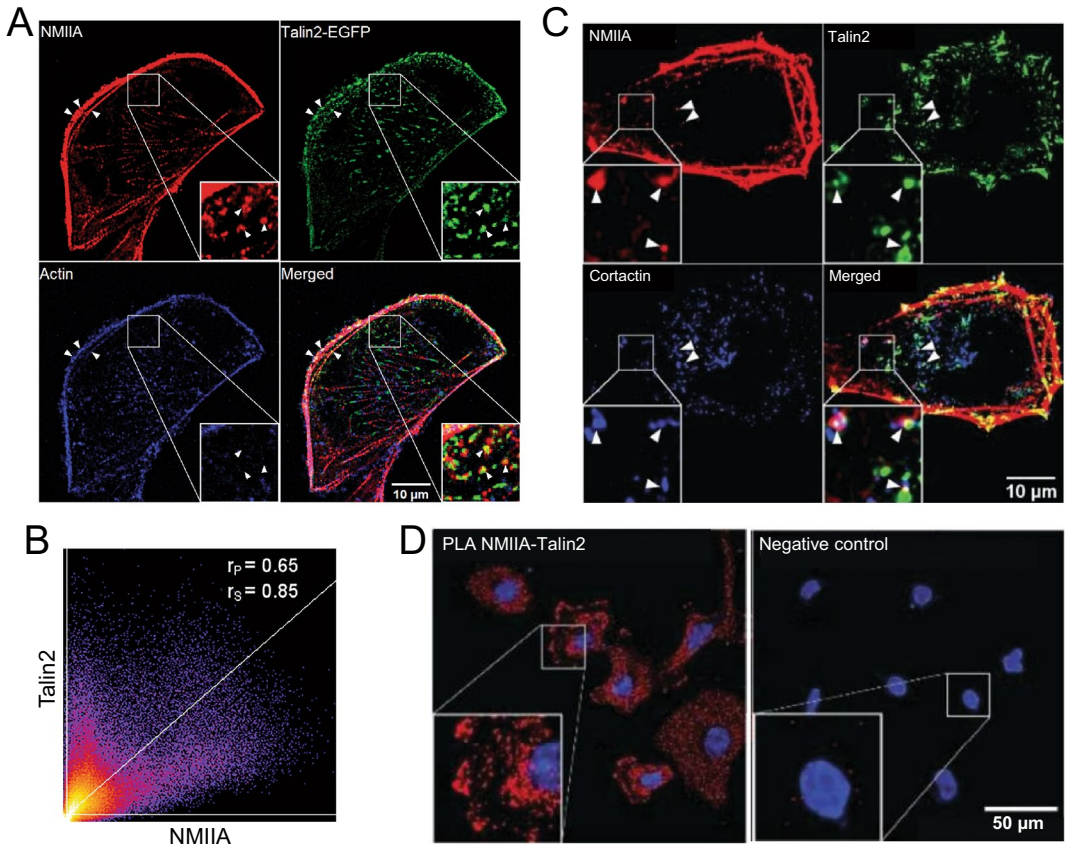

Fig. 4. NMIIA co-localizes with talin2 and cortactin. (**A**) MDA-MB-231 cells were transfected with EGFP-talin2, plated on coverslips precoated with FN. The cells were fixed and NMIIA and F-actin were stained with an anti-NMIIA rabbit polyclonal antibody and Alexa-633 phalloidin. Images were acquired with confocal microscopy. Arrowheads point to the sites of co-localization. (**B**) A 2D colocalization histogram between NMIIA and talin2 staining. The Pearson and Spearman colocalization coefficients are shown. The analysis was based on 20 cells from two independent experiments. (**C**) MDA-MB-231 cells were transfected with EGFP-talin2, and plated on coverslips precoated with laminin. NMIIA and cortactin were stained with an anti-NMIIA rabbit antibody and an anti-cortactin mouse antibody. Arrowheads point to the sites of co-localization. (**D**) MDA-MB-231 cells were plated on coverslips precoated with FN, fixed and incubated with an anti-NMIIA rabbit polyclonal antibody and an anti-talin2 mouse monoclonal antibody (anti-talin2 mouse monoclonal antibody in control sample). The NMIIA-talin2 proximity was detected with a DuoLink PLA assay kit. Red dots, NMIIA-talin2 interactions; blue, nuclei.

(Supplementary Fig. S7), suggesting that talin2 and NMIIA are co-expressed in these cancer tissues, and may function together.

Discussion

In this study, we demonstrate that NMIIA binds to talin2 through its N-terminus and co-localizes with talin2 in cells, implying that NMIIA may mediate the force generation by directly binding to talin2. NMIIA is the major myosin involved in traction force generation[19,20]. The dogma on force generation is that talin interacts with β-integrin tails and F-actin through its head and rod domains, respectively, thus transmitting force from the actin cytoskeleton to the extracellular matrix[24,25]. Talin2 is distinct from talin1 in several aspects: (1) the binding of talin2 to β-integrins is stronger than that of talin1; (2) talin2 localizes in large focal adhesions, while talin1 is found in smaller ones; (3) talin2 mediates traction force through its strong integrin interaction, while talin1 does so by increasing cell adhesions[11,45]. These studies point to the key role of talin2 in cellular force generation. NMIIA interacts with the F_3 subdomain of the talin2 head through its N-terminus, while it does not efficiently bind to talin1 (Figs. 2, 3). Thus, NMIIA could mediate the force generation by binding to talin2, which could be a new paradigm by which NMIIA mediates force generation.

On the other hand, the typical talin2/NMIIA in MDA-MB-231 cells was not observed in either talin1- or talin2-re-expressed TLN1$^{-/-}$ TLN2$^{-/-}$ MKF cells, probably because the expression level of NMIIA in the talin1/talin2 KO MKF cells is lower than that in MDA-MB-231 cells. MYH9 is overexpressed in specimens of different cancer types, including pancreatic cancer, metastatic triple-negative breast cancer, esophageal squamous cell carcinoma, non-small cell lung cancer (NSCLC), stomach cancer, and liver cancer (Supplementary Fig. S6)[27,46–50],

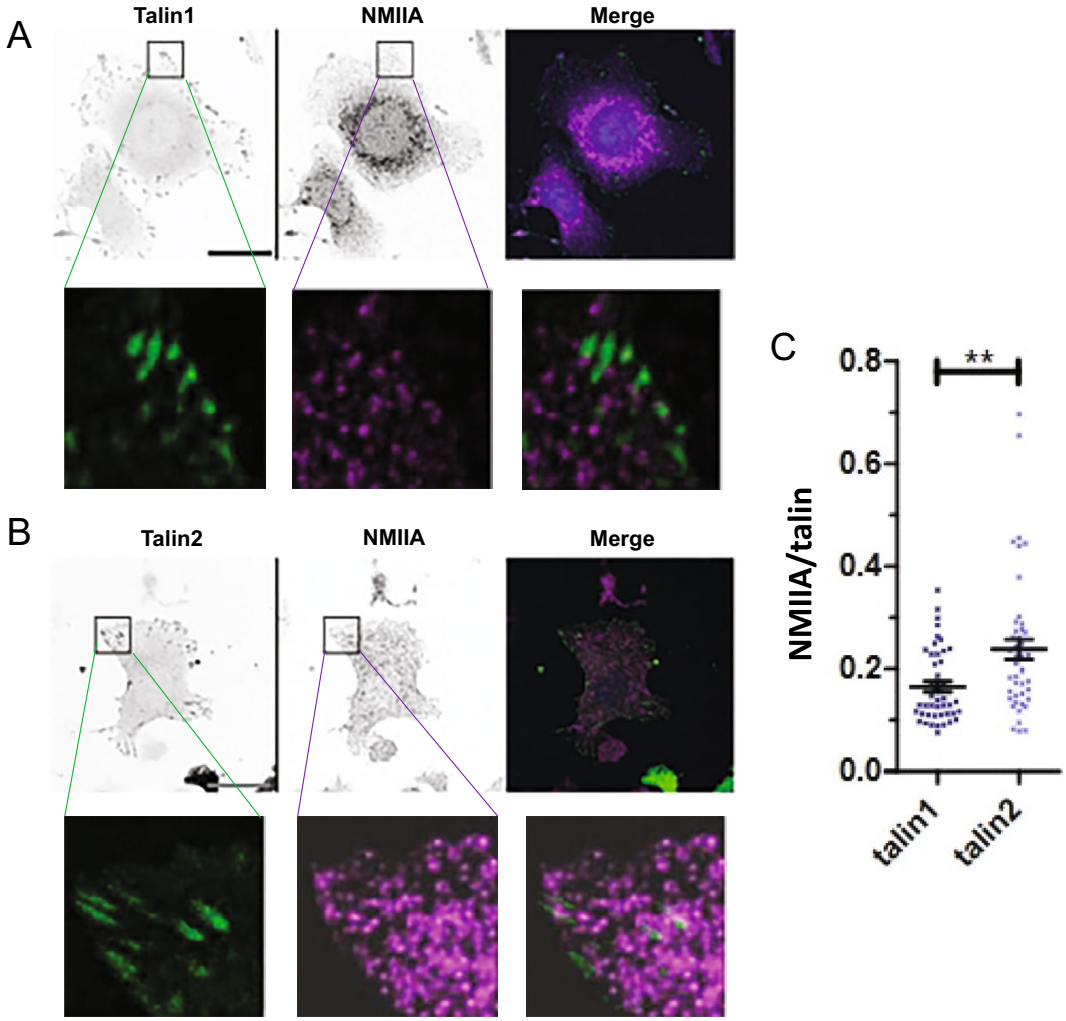

Fig. 5. The distribution of talin1, talin2 and NMIIA in talin1- or talin2-rescued TLN1$^{-/-}$ TLN2$^{-/-}$ MKF cells. The TLN1$^{-/-}$ TLN2$^{-/-}$ MKF cells were transfected with talin1-YPet (A) or talin2-YPet (B) and then stained with an anti-NMIIA rabbit polyclonal antibody. The distribution of talin1 and NMIIA in talin1-YPet-rescued cells (**A**) or distribution of talin2 and NMIIA in talin2-YPet-rescued cells (**B**) were examined with confocal microscopy. The ratio of NMIIA intensity to talin1 and talin2 intensity in adhesion sites was analyzed as described in the Methods section (**C**). Data are from 46 cells per condition (one data point represents one cell; 3 independent experiments pooled; more than 10 adhesions per cell were analyzed and averaged). Scale bars are 25 μm. $P < 0.01$.

and the expression levels are inversely correlated with clinical outcomes. It is thus possible that the talin2-NMIIA axis prevails only in MYH9 highly expressed cancer cells.

Talin1 seems to bind to NMIIA as well, although much weaker compared to talin2 (Fig. 2A). It has been reported that talin1 is overexpressed in ovarian serous carcinoma and oral squamous cell carcinoma[51,52]. Thus, it is likely that NMIIA may bind to talin1 to modulate its biological function in tissues and cells having high talin1 expression.

NMIIA may mediate integrin activation by directly binding to talin2. Talin binding to β-integrin tails is the final common step in integrin activation[1,6]. However, the F_3 subdomain of the talin head domain interacts with the R9 subdomain in the talin rod domain, thus inhibiting talin binding to integrins and integrin activation[53,54]. It has been shown that mechanical forces mediate integrin activation[21,23,24], as well as that mechanical forces can uncover the vinculin-binding sites on the talin rod domain[55–59]. However, it is unknown if forces regulate the intramolecular-interaction between the talin head and rod domains, which prevents talin from binding to β-integrin tails. We showed here that NMIIA interacts with the F_3 subdomain of the talin2 head through its N-terminus (Fig. 3). Also, expression of NMIIA promoted talin2 binding to the β-integrin tail (Fig. 6). Furthermore, depletion of NMIIA in U2 OS cells inhibited cell adhesions on FN (Fig. 6), and expression of truncated mutant NMIIA$_{\Delta 214–1897}$ in U2 OS cells activated the β1 integrin, whereas that of NMIIA$_{\Delta 1–1813}$ inhibited integrin activation (Fig. 7), probably through disrupting force generation or cargo transportation that require for integrin activation, suggesting a role of NMIIA in integrin activation. NMIIA could therefore activate β1 integrins by

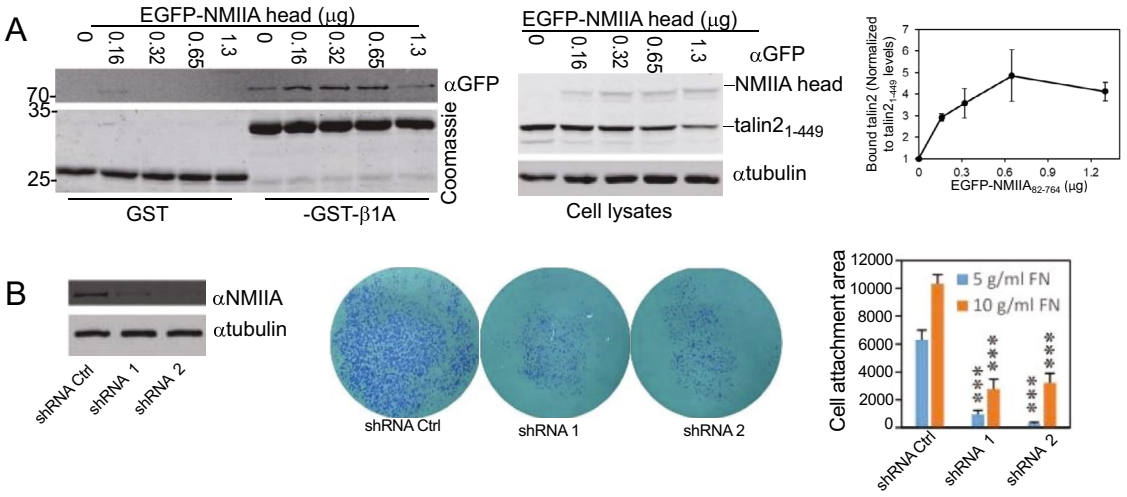

Fig. 6. NMIIA promotes the talin2-β-integrin interaction and regulates cell adhesions. (**A**) EGFP-talin2$_{1-449}$ (0.2 μg plasmid) was co-transfected with different amounts of EGFP-NMIIA head plasmid as indicated into CHO-K1 cells. The interaction of talin2$_{1-449}$ with the β1A tails was examined by GST-β1A tail pulldown assays, using GST as a control. Bound talin2$_{1-449}$ was normalized to its expression levels in cell lysates. The results represent Mean ± SD from three independent binding assays using cell lysates from the same transfections. (**B**) NMIIA-depleted U2 OS cells in serum-free medium were plated on FN (5, 10 μg/ml)-coated 96-well plates for 60 min, using shRNA control cells as a control. Unattached cells were washed away with PBS, and attached cells were fixed and stained with crystal violet. Data are presented as mean ± SD. N = 4, $^{***}P < 0.001$.

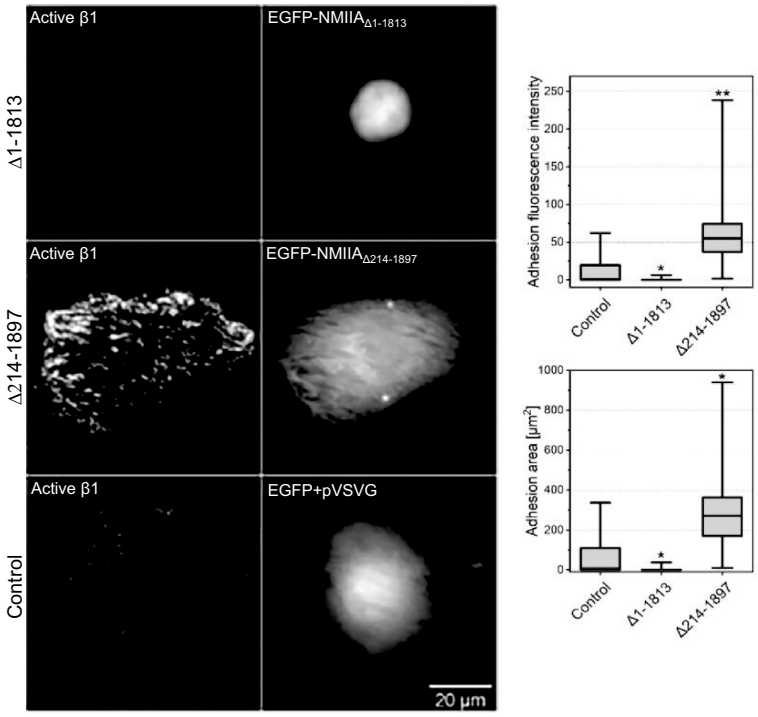

Fig. 7. Expression of truncated NMIIA mutants changes β-integrin activation. U2OS cells were transfected with EGFP-NMIIA$_{Δ1-1813}$, -NMIIA$_{Δ214-1897}$, and EGFP empty vector, respectively, plated on fibronectin-coated glass-bottom dishes, and stained with an anti-active β1-integrin antibody (12G10). Images were acquired with TIRF and Epifluorescence microscopy. Data presented as 10–25–50–75–90 percentiles. 40 cells/group were analyzed. U-test, $^{*}P < 0.05$, $^{**}P < 0.01$.

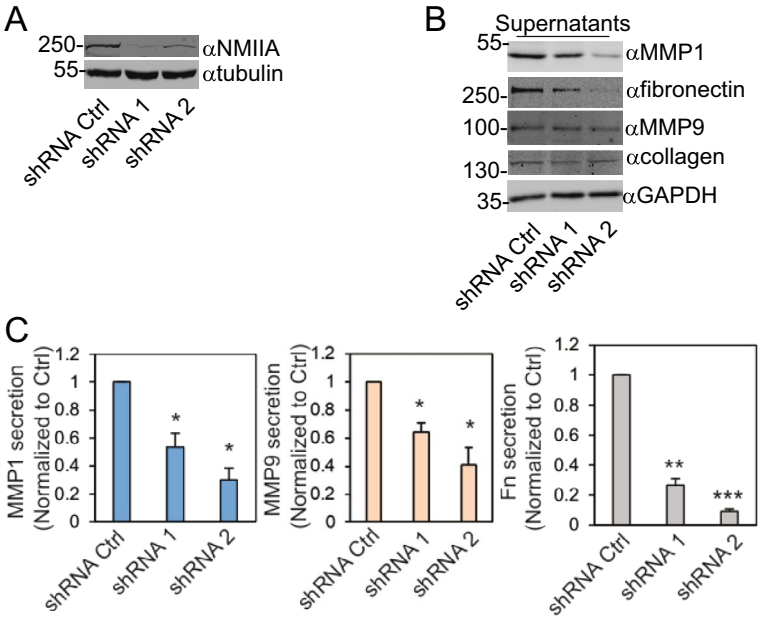

Fig. 8. Depletion of NMIIA inhibited FN and MMP secretion. (**A**) Expression levels of NMIIA in NMIIA-depleted MDA-MB-231 cells and control cells. (**B**) NMIIA-depleted and control MDA-MB-231 cells were cultured in serum-free DMEM media for 24 h. The conditioned media (CM) were collected and concentrated. MMP1, MMP9, FN, collagen I, and GAPDH in the CM were detected using Western blotting. (**C**) The levels of MMP1, MMP9, and FN in CM. Data represent mean ± SD. n = 3.

binding to the F3 subdomain of the talin2 head, and consequently disrupting the intramolecular interaction and activating talin2.

Previously we demonstrated that talin2-mediated traction force plays an essential role in cell invasion by modulating MMP secretion[11]. We thought that the binding of talin2 to NMIIA could modulate MMP secretion. However, depletion of NMIIA in MDA-MB-231 cells had only a partial inhibition on MMP1 and MMP9 secretion (Fig. 8). Since myosin-X and talin activate integrin at filopodia tips[60], it is possible that talin2 may interact with myosin-X, a homolog of NMIIA implicated in the secretion of MMP2 and MMP9 and cell invasion[61], to mediate MMP secretion as well, while bind to NMIIA to modulate integrin activation and cell adhesion.

We previously showed that talin2 bound to β-integrin tails more strongly than talin1[11]. However, when purified talin1 and talin2 interacted with the β integrin tail, the affinity of talin2 with the β integrin tail was only slightly stronger than that of talin1[17], suggesting that other proteins in cell lysates may promote talin2 binding to the β integrin tail. This hypothesis is supported by the finding that over-expression of the NMIIA head domain promotes talin2 binding to the β integrin tail (Fig. 6). Thus, NMIIA could be a promoter of the talin2-β-integrin interaction and subsequent integrin activation. Further studies are needed for understanding the role of NMIIA in integrin activation.

Since talin2 plays an essential role in tumor growth and metastasis, and both talin2 and NMIIA are up-regulated in multiple cancer types, including pancreatic adenocarcinoma, prostate cancer and stomach adenocarcinoma (Supplementary Figs. S1 and S6), it is quite possible that the interaction of talin2 with NMIIA regulates integrin activation and consequently tumor growth and metastasis. Thus, the talin2-NMIIA interaction could be a potential target for cancer therapy. We previously showed that cyanidin-3-glucoside bound to talin2 at region potentially involved in the talin2/NMIIA interaction, and that it promoted the talin-β-integrin interaction and cell adhesion[62]. This suggests that the talin2/NMIIA interaction may be targetable by small compounds, leading to novel anti-cancer therapies.

Data availability

All data is included in the manuscript figures or supplementary information file.

Received: 11 March 2024; Accepted: 22 August 2024
Published online: 30 August 2024

References

1. Tadokoro, S. *et al.* Talin binding to integrin ß tails: A final common step in integrin activation. *Science* **302**, 103–106. https://doi.org/10.1126/science.1086652 (2003).
2. Ratnikov, B. I., Partridge, A. W. & Ginsberg, M. H. Integrin activation by talin. *J. Thromb. Haemost.* **3**, 1783–1790. https://doi.org/10.1111/j.1538-7836.2005.01362.x (2005).
3. Huang, C. *et al.* Talin phosphorylation by Cdk5 regulates Smurf1-mediated talin head ubiquitylation and cell migration. *Nat. Cell Biol.* **11**, 624–630. https://doi.org/10.1038/ncb1868 (2009).

4. Goult, B. T. *et al.* RIAM and vinculin binding to talin are mutually exclusive and regulate adhesion assembly and turnover. *J. Biol. Chem.* **288**, 8238–8249. https://doi.org/10.1074/jbc.M112.438119 (2013).
5. Nuckolls, G. H., Turner, C. E. & Burridge, K. Functional studies of the domains of talin. *J. Cell Biol.* **110**, 1635–1644. https://doi.org/10.1083/jcb.110.5.1635 (1990).
6. Calderwood, D. A. *et al.* The talin head domain binds to integrin β subunit cytoplasmic tails and regulates integrin activation. *J. Biol. Chem.* **274**, 28071–28074. https://doi.org/10.1074/jbc.274.40.28071 (1999).
7. Atherton, P. *et al.* Vinculin controls talin engagement with the actomyosin machinery. *Nat. Commun.* **6**, 10038. https://doi.org/10.1038/ncomms10038 (2015).
8. Gingras, A. R. *et al.* Mapping and consensus sequence identification for multiple vinculin binding sites within the Talin Rod. *J. Biol. Chem.* **280**, 37217–37224. https://doi.org/10.1074/jbc.M508060200 (2005).
9. Hemmings, L. *et al.* Talin contains three actin-binding sites each of which is adjacent to a vinculin-binding site. *J. Cell Sci.* **109**, 2715–2726. https://doi.org/10.1242/jcs.109.11.2715 (1996).
10. Praekelt, U. *et al.* New isoform-specific monoclonal antibodies reveal different sub-cellular localisations for talin1 and talin2. *Eur. J. Cell Biol.* **91**, 180–191. https://doi.org/10.1016/j.ejcb.2011.12.003 (2012).
11. Qi, L. *et al.* Talin2-mediated traction force drives matrix degradation and cell invasion. *J. Cell Sci.* **129**, 3661–3674. https://doi.org/10.1242/jcs.185959 (2016).
12. Senetar, M. A., Moncman, C. L. & McCann, R. O. Talin2 is induced during striated muscle differentiation and is targeted to stable adhesion complexes in mature muscle. *Cell Motil. Cytoskelet.* **64**, 157–173. https://doi.org/10.1002/cm.20173 (2007).
13. Huet-Calderwood, C., Rivera-Molina, F. E., Toomre, D. K. & Calderwood, D. A. Fibroblasts secrete fibronectin under lamellipodia in a microtubule- and myosin II–dependent fashion. *J. Cell Biol.* **222**, e202204100. https://doi.org/10.1083/jcb.202204100 (2023).
14. Li, L. *et al.* The role of talin2 in breast cancer tumorigenesis and metastasis. *Oncotarget* **8**, 106876–106887. https://doi.org/10.18632/oncotarget.22449 (2017).
15. Austen, K. *et al.* Extracellular rigidity sensing by talin isoform-specific mechanical linkages. *Nat. Cell Biol.* **17**, 1597–1606. https://doi.org/10.1038/ncb3268 (2015).
16. Anthis, N. J., Wegener, K. L., Critchley, D. R. & Campbell, I. D. Structural diversity in integrin/talin interactions. *Structure* **18**, 1654–1666. https://doi.org/10.1016/j.str.2010.09.018 (2010).
17. Yuan, Y. *et al.* The molecular basis of talin2's high affinity toward β1-integrin. *Sci. Rep.* **7**, 41989. https://doi.org/10.1038/srep41989 (2017).
18. Baster, Z., Li, L., Rajfur, Z. & Huang, C. Talin2 mediates secretion and trafficking of matrix metallopeptidase 9 during invadopodium formation. *Biochim. Biophys. Acta Mol. Cell Res.* **1867**, 118693. https://doi.org/10.1016/j.bbamcr.2020 (2020).
19. Cai, Y. *et al.* Nonmuscle myosin IIA-dependent force inhibits cell spreading and drives F-actin flow. *Biophys. J.* **91**, 3907–3920. https://doi.org/10.1529/biophysj.106.084806 (2006).
20. Jorrisch, M. H., Shih, W. & Yamada, S. Myosin IIA deficient cells migrate efficiently despite reduced traction forces at cell periphery. *Biol.Open* **2**, 368–372. https://doi.org/10.1242/bio.20133707 (2013).
21. Katsumi, A., Naoe, T., Matsushita, T., Kaibuchi, K. & Schwartz, M. A. Integrin activation and matrix binding mediate cellular responses to mechanical stretch. *J. Biol. Chem.* **280**, 16546–16549. https://doi.org/10.1074/jbc.C400455200 (2005).
22. Friedland, J. C., Lee, M. H. & Boettiger, D. Mechanically activated integrin switch controls alpha5beta1 function. *Science* **323**, 642–644. https://doi.org/10.1126/science.1168441 (2009).
23. Chen, W., Lou, J., Evans, E. A. & Zhu, C. Observing force-regulated conformational changes and ligand dissociation from a single integrin on cells. *J. Cell Biol.* **199**, 497–512. https://doi.org/10.1083/jcb.201201091 (2012).
24. Sun, Z., Costell, M. & Fässler, R. Integrin activation by talin, kindlin and mechanical forces. *Nat. Cell Biol.* **21**, 25–31. https://doi.org/10.1038/s41556-018-0234-9 (2019).
25. Elosegui-Artola, A. *et al.* Mechanical regulation of a molecular clutch defines force transmission and transduction in response to matrix rigidity. *Nat. Cell Biol.* **18**, 540–548. https://doi.org/10.1038/ncb3336 (2016).
26. Lin, X. *et al.* Silencing MYH9 blocks HBx-induced GSK3β ubiquitination and degradation to inhibit tumor stemness in hepatocellular carcinoma. *Signal Transduct. Target Ther.* **5**, 13. https://doi.org/10.1038/s41392-020-0111-4 (2020).
27. Liu, D. *et al.* Clinicopathological significance of NMIIA overexpression in human gastric cancer. *Int. J. Mol. Sci.* **13**, 15291–15304. https://doi.org/10.3390/ijms131115291 (2012).
28. Wang, Z. *et al.* NMIIA promotes tumorigenesis and prevents chemosensitivity in colorectal cancer by activating AMPK/mTOR pathway. *Exp. Cell Res.* **398**, 112387. https://doi.org/10.1016/j.yexcr.2020.112387 (2021).
29. Xiong, D. *et al.* The overexpression of NMHC IIA promoted invasion and metastasis of nasopharyngeal carcinoma cells. *J. Cancer* **12**, 4218–4228. https://doi.org/10.7150/jca.47506 (2021).
30. Yang, B. *et al.* MYH9 promotes cell metastasis via inducing angiogenesis and epithelial mesenchymal transition in esophageal squamous cell carcinoma. *Int. J. Med. Sci.* **17**, 2013–2023. https://doi.org/10.7150/ijms.46234 (2020).
31. Zhong, Y. *et al.* MYH9-dependent polarization of ATG9B promotes colorectal cancer metastasis by accelerating focal adhesion assembly. *Cell Death Differ.* **28**, 3251–3269. https://doi.org/10.1038/s41418-021-00813-z (2021).
32. Wei, Q. & Adelstein, R. S. Conditional expression of a truncated fragment of nonmuscle myosin II-A alters cell shape but not cytokinesis in HeLa cells. *Mol. Biol. Cell* **11**, 3617–3627. https://doi.org/10.1091/mbc.11.10.3617 (2020).
33. Theodosiou, M. *et al.* Kindlin-2 cooperates with talin to activate integrins and induces cell spreading by directly binding paxillin. *Elife* **5**, e10130. https://doi.org/10.7554/eLife.10130 (2016).
34. Wu, Z. *et al.* PIPKIγ regulates focal adhesion dynamics and colon cancer cell invasion. *PLoS ONE* **6**, e24775. https://doi.org/10.1371/journal.pone.0024775 (2011).
35. Li, X. *et al.* Ubiquitylation of phosphatidylinositol 4-phosphate 5-kinase type I γ by HECTD1 regulates focal adhesion dynamics and cell migration. *J. Cell Sci.* **126**, 2617–2628. https://doi.org/10.1242/jcs.117044 (2013).
36. Schindelin, J. *et al.* Fiji: An open-source platform for biological-image analysis. *Nat. Methods* **9**, 676–682. https://doi.org/10.1038/nmeth.2019 (2012).
37. Baster, Z. & Rajfur, Z. BatchDeconvolution: A Fiji plugin for increasing deconvolution workflow. *Bio Algorithms Med Syst.* **16**, 20200027. https://doi.org/10.1515/bams-2020-0027 (2020).
38. Tang, G., Cho, M. & Wang, X. OncoDB: An interactive online database for analysis of gene expression and viral infection in cancer. *Nucleic Acids Res.* **50**(D1), D1334–D1339. https://doi.org/10.1093/nar/gkab970 (2022).
39. Liang, Y. *et al.* Talin2 regulates breast cancer cell migration and invasion by apoptosis. *Oncol. Lett.* **16**, 285–293. https://doi.org/10.3892/ol.2018.8641 (2018).
40. Wen, Z. *et al.* Talin2 regulates invasion of human breast cancer MDA-MB-231 cells via alteration of the tumor microenvironment. *Oncol. Lett.* **17**, 4835–4842. https://doi.org/10.3892/ol.2019.10175 (2019).
41. Fujita-Becker, S. *et al.* Functional characterization of the N-terminal region of myosin-2. *J. Biol. Chem.* **281**, 36102–36109. https://doi.org/10.1074/jbc.M605171200 (2006).
42. Pecci, A., Ma, X., Savoia, A. & Adelstein, R. S. MYH9: Structure, functions and role of non-muscle myosin IIA in human disease. *Gene* **664**, 152–167. https://doi.org/10.1016/j.gene.2018.04.048 (2018).
43. Artym, V. V., Zhang, Y., Seillier-Moiseiwitsch, F., Yamada, K. M. & Mueller, S. C. Dynamic interactions of cortactin and membrane type 1 matrix metalloproteinase at invadopodia: Defining the stages of invadopodia formation and function. *Cancer Res.* **66**, 3034–3043. https://doi.org/10.1158/0008-5472.CAN-05-2177 (2006).

44. Jeannot, P. & Besson, A. Cortactin function in invadopodia. *Small GTPases* **11**, 256–270. https://doi.org/10.1080/21541248.2017.1405773 (2020).
45. Qi, L., Kolodziej, T., Rajfur, Z. & Huang, C. Roles of talin2 in traction force generation, tumor metastasis and cardiovascular integrity. *Curr. Protein Pept. Sci.* **19**, 1071–1078. https://doi.org/10.2174/1389203719666180809094731 (2018).
46. Balouchi-Anaraki, S., Ahmadvand, S., Safaei, A. & Ghaderi, A. 4H12, a murine monoclonal antibody directed against myosin heavy chain-9 expressed on acinar cell carcinoma of pancreas with potential therapeutic application. *Iran. Biomed. J.* **25**, 310–322. https://doi.org/10.52547/ibj.25.5.310 (2021).
47. Lund, R. R. *et al.* Quantitative proteomics of primary tumors with varying metastatic capabilities using stable isotope-labeled proteins of multiple histogenic origins. *Proteomics* **12**, 2139–2148. https://doi.org/10.1002/pmic.201100490 (2012).
48. Xia, Z. K. *et al.* Nonmuscle myosin IIA is associated with poor prognosis of esophageal squamous cancer. *Dis. Esophagus* **25**, 427–436. https://doi.org/10.1111/j.1442-2050.2011.01261.x (2012).
49. Katono, K. *et al.* Prognostic significance of MYH9 expression in resected non-small cell lung cancer. *PLoS ONE* **10**, e0121460. https://doi.org/10.1371/journal.pone.0121460 (2015).
50. Lin, X., Yu, G. F., Zuo, S., Luo, R. C. & Fang, W. Y. Low MYH9 expression predicts a good prognosis for hepatocellular carcinoma. *Int. J. Clin. Exp. Pathol.* **11**, 2784–2791 (2018).
51. Lai, M. T. *et al.* Talin-1 overexpression defines high risk for aggressive oral squamous cell carcinoma and promotes cancer metastasis. *J. Pathol.* **224**, 367–376. https://doi.org/10.1002/path.2867 (2011).
52. Sharbatoghli, M. *et al.* The association between higher expression of talin-1 and the reduced survival rate in ovarian serous carcinoma patients. *Iran. J. Pathol.* **18**, 312–326. https://doi.org/10.30699/IJP.2023.554227.2901 (2023).
53. Goksoy, E. *et al.* Structural basis for the autoinhibition of talin in regulating integrin activation. *Mol. Cell* **31**, 124–133. https://doi.org/10.1016/j.cell.2019.08.034 (2008).
54. Zhang, H., Chang, Y.-C., Huang, Q., Brennan, M. L. & Wu, J. Structural and functional analysis of a talin triple-domain module suggests an alternative talin autoinhibitory configuration. *Structure* **24**, 721–729. https://doi.org/10.1016/j.str.2016.02.020 (2016).
55. Jiang, G., Giannone, G., Critchley, D. R., Fukumoto, E. & Sheetz, M. P. Two-piconewton slip bond between fibronectin and the cytoskeleton depends on talin. *Nature* **424**, 334–337. https://doi.org/10.1038/nature01805 (2003).
56. Hytönen, V. P. & Vogel, V. How force might activate talin's vinculin binding sites: SMD reveals a structural mechanism. *PLoS Comput. Biol.* **4**, e24. https://doi.org/10.1371/journal.pcbi.0040024 (2008).
57. del Rio, A. *et al.* Stretching single talin rod molecules activates vinculin binding. *Science* **323**, 638–641. https://doi.org/10.1126/science.1162912 (2009).
58. Yao, M. *et al.* Mechanical activation of vinculin binding to talin locks talin in an unfolded conformation. *Sci. Rep.* **4**, 4610. https://doi.org/10.1038/srep04610 (2014).
59. Yao, M. *et al.* The mechanical response of talin. *Nat. Commun.* **7**, 11966. https://doi.org/10.1038/ncomms11966 (2016).
60. Miihkinen, M. *et al.* Myosin-X and talin modulate integrin activity at filopodia tips. *Cell Rep.* **36**, 109716. https://doi.org/10.1016/j.celrep.2021.109716 (2021).
61. Deng, G., Fu, T.-J. & Liu, C.-P. Increased expression of Myosin X contributes to the metastasis in patients with laryngeal squamous cell carcinoma. *Mol. Genet. Genomics* **297**, 1529–1536. https://doi.org/10.1007/s00438-022-01934-x (2022).
62. Baster, Z. *et al.* Cyanidin-3-glucoside binds to talin and modulates colon cancer cell adhesions and 3D growth. *FASEB J.* **34**, 2227–2237. https://doi.org/10.1096/fj.201900945R (2020).

Author contributions

X.W. performed OncoDB database mining, computational modeling, data analysis and paper writing, Z.B. carried out experiments and data analysis, L.A. performed experiments and paper writing, L.L. performed experiments, Z.R. and V.P.H. discussed and edited the manuscript, C.H. directed the study and wrote the manuscript. All authors contributed to the article and approved the submitted version.

Funding

This work was partially supported by National Institutes of Health Grant R01 GM122994 (to CH), Academy of Finland Grant 331946 (to VH), Cancer Society of Finland (to VH) and Sigrid Juselius Foundation (to VH). ZB's work was supported by the Polish National Science Centre PRELUDIUM Grant No. 2018/31/N/ NZ3/02031.

Competing interests

The authors declare no competing interests.

Additional information

Supplementary Information The online version contains supplementary material available at https://doi.org/10.1038/s41598-024-70866-w.

Correspondence and requests for materials should be addressed to X.W., V.P.H. or C.H.